

Bilayered $\text{Mg}_{0.25}\text{V}_2\text{O}_5\cdot\text{H}_2\text{O}$ as a Stable Cathode for Rechargeable Ca-Ion Batteries

Xiaoming Xu,^{†,‡} Manyi Duan,^{‡,‡} Yunfan Yue,[†] Qi Li,[†] Xiao Zhang,[†] Lu Wu,[†] Peijie Wu,[†] Bo Song^{*,§} and Liqiang Mai^{*,†}

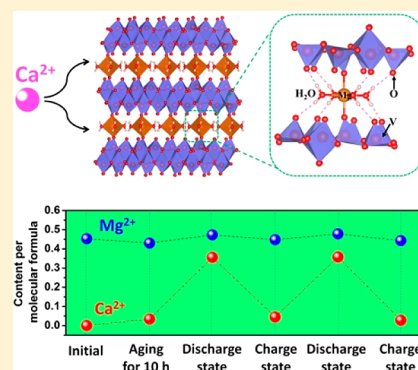
[†]State Key Laboratory of Advanced Technology for Materials Synthesis and Processing, Wuhan University of Technology, Wuhan 430070, People's Republic of China

[‡]College of Physics and Electronic Engineering, Sichuan Normal University, Chengdu 610101, China

[§]Terahertz Technology Innovation Research Institute, School of Optical–Electrical Computer Engineering, University of Shanghai for Science and Technology, Shanghai 200093, China

S Supporting Information

ABSTRACT: The calcium-ion battery is an emerging energy storage system that has attracted considerable attention recently. However, the absence of high-performance cathode materials is one of the main challenges for the development of calcium-ion batteries. Herein, a bilayered $\text{Mg}_{0.25}\text{V}_2\text{O}_5\cdot\text{H}_2\text{O}$ as a stable cathode for rechargeable calcium-ion batteries is identified. Remarkably, an unexpected stable structure of the material for Ca^{2+} storage is demonstrated. It is found that the interlayer spacing shows only a tiny variation of ~ 0.09 Å during Ca^{2+} insertion/extraction, which results in its outstanding cycling stability (capacity retention of 86.9% after 500 cycles) for Ca^{2+} storage. On the basis of in situ/ex situ experimental characterizations and ab initio simulation, the origin of such superior structural stability is revealed. This ultrastable cathode together with the understanding lays a strong foundation for developing high-performance calcium-ion batteries.



Multivalent metal-ion batteries have recently attracted extensive interest toward next-generation energy storage devices because of their potential for higher capacity with lower cost and better safety compared to the present commercialized lithium-ion batteries.^{1,2} Magnesium-ion batteries,^{3–5} zinc-ion batteries,^{6–9} and aluminum-ion batteries^{10–12} have received much attention with significant progress in the past few years. In comparison, calcium-ion batteries (CIBs), as another multivalent-ion battery, have been relatively less studied until now.¹³ However, in principle, the standard reduction potential of calcium (-2.87 V vs standard hydrogen electrode (SHE)) is closest to that of lithium (-3.04 V vs SHE) when compared to magnesium (-2.37 V vs SHE), zinc (-0.76 V vs SHE), and aluminum (-1.66 V vs SHE), which suggests a higher output voltage of CIBs than other multivalent-ion batteries.¹ Besides, because of the larger ionic radius, Ca^{2+} ions show smaller charge density and thus smaller polarization strength compared with Mg^{2+} , Zn^{2+} , and Al^{3+} ions (as shown in Figure S1), indicating that Ca^{2+} ions may have better diffusion kinetics among the multivalent charge carriers.^{13–15} These two merits together with the high abundance of calcium resource¹⁶ determine that CIBs are a promising battery system for the future.

The development of CIBs mainly suffers from two challenges: one is irreversible calcium plating/stripping for

metallic calcium in various electrolytes, which seriously hinders fundamental research about CIBs based on calcium metal anodes; the other is the lack of high-performance electrode materials for Ca^{2+} storage.^{13,17} Since 2015, much important progress has been reported about CIBs. Ponrouch et al. demonstrated that calcium plating/stripping is feasible at high temperatures (75 and 100 °C).¹⁸ After that, Bruce's group further identified an organic electrolyte, $\text{Ca}(\text{BH}_4)_2$ in tetrahydrofuran, that enables calcium plating/stripping at room temperature.¹⁹ In terms of electrode materials, utilization of Sn metal and a mesocarbon microbead as Ca^{2+} storage anodes with good cycling stability has been proposed by Tang and coauthors very recently.^{20,21} However, for cathode research, even though several cathode materials for Ca^{2+} storage have been reported, the performance, especially the cycling stability, is still far from being satisfactory.^{22–30} As far as we know, the cycling performance of the reported CIB cathodes seldom exceeds 100 cycles. Due to the divalent property and relatively large ionic radius of Ca^{2+} ions, searching for suitable cathode materials with a large diffusion

Received: April 17, 2019

Accepted: May 15, 2019

Published: May 15, 2019

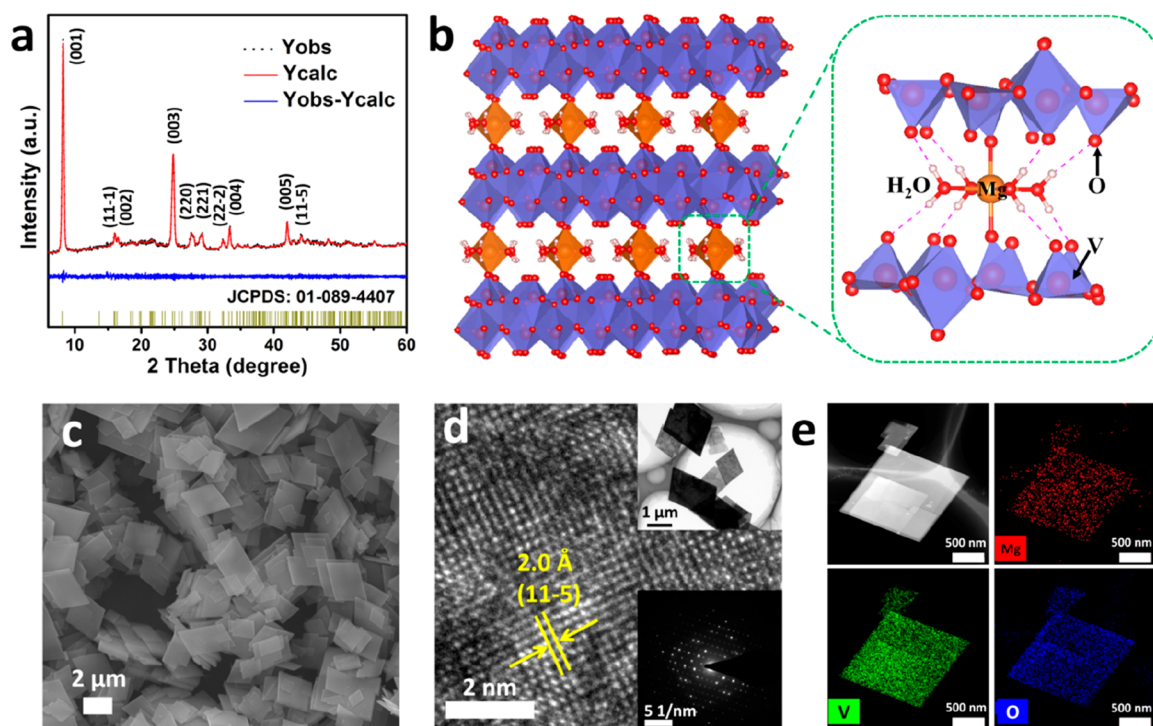


Figure 1. Structure and morphology characterizations of the as-synthesized $\text{Mg}_{0.25}\text{V}_2\text{O}_5\cdot\text{H}_2\text{O}$. (a) XRD pattern and Rietveld refinement; (b) crystal structure; (c) SEM image; (d) HRTEM image; the insets are the TEM image and SAED pattern; and (e) EDX mapping.

channel and good structural stability is very important for the development of rechargeable CIBs.

Herein, we identified a bilayered $\text{Mg}_{0.25}\text{V}_2\text{O}_5\cdot\text{H}_2\text{O}$ (MVOH) with large interlayer spacing of 10.76 Å as a high-performance CIB cathode. The large interlayer spacing provides sufficient space for Ca^{2+} ion diffusion. The crystal water in the interlayers could provide a charge screening effect.^{31,32} More importantly, we demonstrated that this material shows unexpected structural stability during Ca^{2+} ion insertion and extraction, with an interlayer spacing variation of only ~ 0.09 Å. Such a tiny variation results in excellent cycling stability up to 500 cycles, which is the best cycling performance among the reported CIB cathodes, to the best of our knowledge.

Characterization of the obtained material is shown in Figure 1. The X-ray diffraction (XRD) pattern and further Rietveld refinement (Figure 1a) indicate that the obtained phase matches very well with $\text{Mg}_{0.25}\text{V}_2\text{O}_5\cdot\text{H}_2\text{O}$ (JCPDS: 01-089-4407). The Rietveld refinement parameters indicate that the material is a monoclinic structure with lattice parameters of $a = 10.761$ Å, $b = 16.253$ Å, $c = 21.949$ Å, and $\beta = 93.95^\circ$. This phase has a bilayered structure stacking along the c direction, with a large interlayer spacing of ~ 10.76 Å.³³ The bilayered structure is pillared by Mg^{2+} ions and crystal water in the interlayers (Figure 1b). The scanning electron microscope (SEM) image shows a parallelogram-shaped plate (Figure 1c) with a side length of 1–3 μm and thickness of 100–300 nm (Figure S2). Thermogravimetry analysis (TGA) was performed in an Ar atmosphere, and a weight loss of $\sim 8.8\%$ between 150 and 400 °C was observed (Figure S3), which corresponds to evaporation of crystal water.^{7,32} The weight loss of $\sim 8.8\%$ is very consistent with the theoretical water content (8.74%) of $\text{Mg}_{0.25}\text{V}_2\text{O}_5\cdot\text{H}_2\text{O}$. The transmission electron microscopy (TEM) image further manifests the morphology of the sample (Figure 1d, inset). The high-resolution TEM (HRTEM) image displays distinct lattice fringes with spacing

of 2.0 Å (Figure 1d), which can be assigned to the (11–5) plane. The selected area electron diffraction (SAED) pattern with regular diffraction spots indicates the single-crystalline nature of the sample (Figure 1d, inset). Energy dispersive X-ray spectrometry (EDX) mapping demonstrates the uniform distribution of the Mg, V, and O elements (Figure 1e). The X-ray photoelectron spectroscopy (XPS) result indicates the coexistence of V^{4+} and V^{5+} in the material (Figure S4).

The large interlayer spacing of 10.76 Å and the charge screening effect of crystal water indicate that the obtained MVOH is a promising cathode material for multivalent-ion batteries. To investigate the Ca^{2+} storage performance of the obtained material, a Swagelok-type cell (as shown in Figure S5) and three-electrode system were used to perform the electrochemical testing. Aluminum foil was used as the current collector, which was stable and could avoid side reactions, such as a corrosion reaction during charge/discharge,³⁴ as demonstrated later. Activated carbon cloth (ACC) was used as the counter electrode in both the Swagelok-type cell and three-electrode system³⁵ by adsorption/desorption of anions during charge/discharge because metallic calcium was unavailable (the calcium plating/stripping is irreversible for metallic calcium) in most of the electrolytes. The electrolyte was $\text{Ca}(\text{TFSI})_2$ dissolved in quaternary ester carbonates. A Ag^+/Ag reference electrode (Figure S6a) was applied in the three-electrode system. The potential of the Ag^+/Ag reference electrode was calibrated by ferrocene (see details in the Supporting Information, Figure S6b).

Cyclic voltammetry (CV) measurement was first carried out in the voltage range of -1.5 – 1.2 V (vs Ag^+/Ag) at a scan rate of 0.2 mV s^{-1} in the three-electrode system (Figure 2a). During the initial negative scan, no distinct cathodic peak was observed for MVOH. However, in the positive scan, a strong anodic peak at ~ 0.48 V (vs Ag^+/Ag) appeared. The CV curve indicates asymmetric Ca^{2+} intercalation and deintercalation

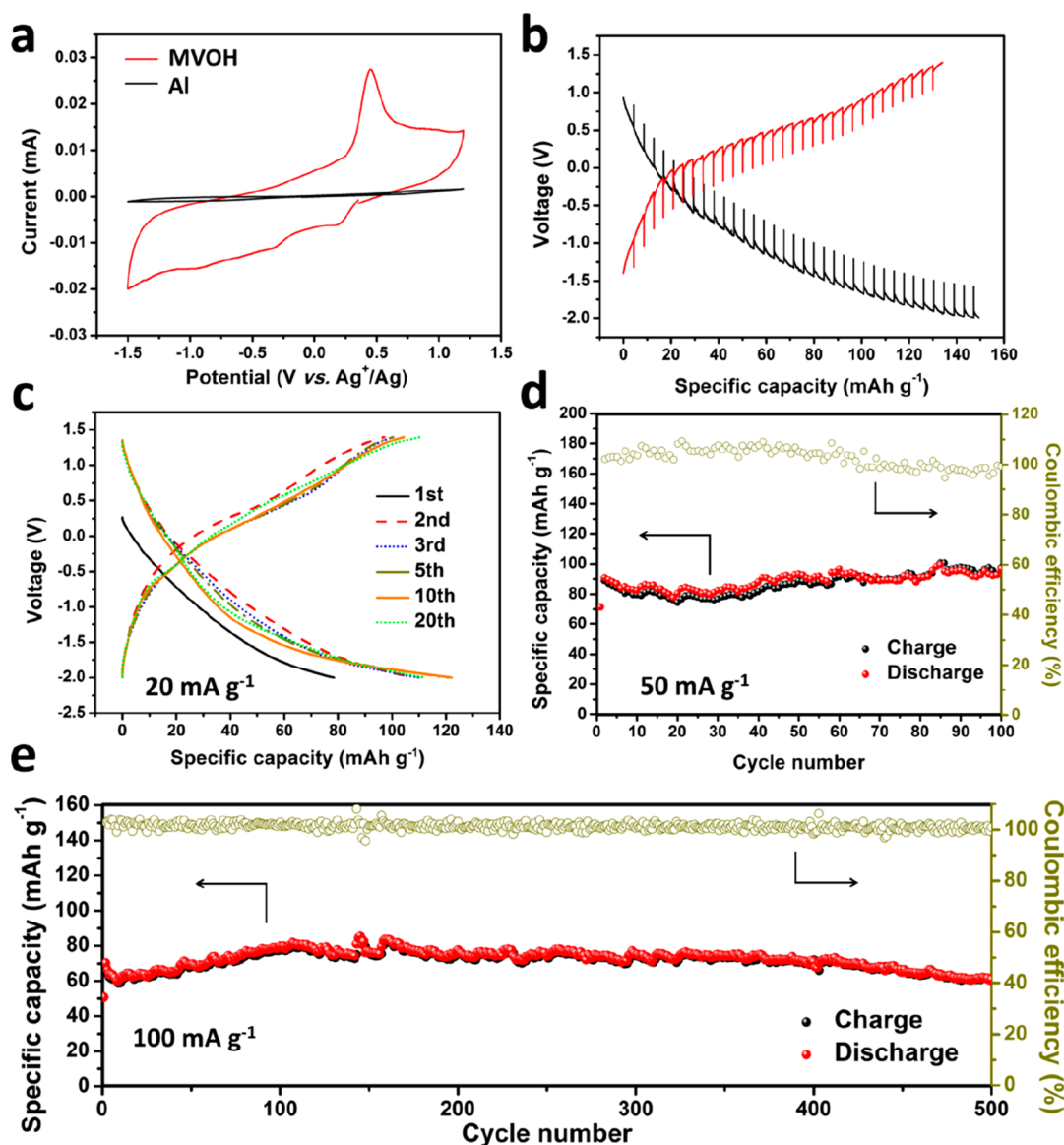


Figure 2. Ca^{2+} storage properties of the as-synthesized $\text{Mg}_{0.25}\text{V}_2\text{O}_5\cdot\text{H}_2\text{O}$. (a) CV curves based on the three-electrode system with ACC as the counter electrode and the Ag^+/Ag electrode as the reference. (b) GITT measurement based on the two-electrode system ($\text{Mg}_{0.25}\text{V}_2\text{O}_5\cdot\text{H}_2\text{O}/\text{ACC}$). (c) Charge/discharge curves of the $\text{Mg}_{0.25}\text{V}_2\text{O}_5\cdot\text{H}_2\text{O}/\text{ACC}$ cell at a current density of 20 mA g^{-1} . (d,e) Cycling performance of $\text{Mg}_{0.25}\text{V}_2\text{O}_5\cdot\text{H}_2\text{O}$ for Ca^{2+} storage based on the two-electrode system at current densities of 50 mA g^{-1} (d) and 100 mA g^{-1} (e).

behavior of MVOH. As far as we know, similar asymmetric behavior has also been observed in several other cathodes for Ca^{2+} storage.^{22,25,36} It suggests a different reaction mechanism between the Ca^{2+} insertion and extraction processes. Besides, CV measurement was also applied to the Al foil (current collect) in the same condition. The voltammogram intensity for Al foil is negligible compared with that of MVOH, indicating that Al foil is adequate as the current collect with no side reaction during the electrochemical process.

Galvanostatic intermittent titration technique (GITT) measurement (Figure 2b) was carried out based on the Swagelok-type cell (MVOH//ACC, voltage range of -2.0 – 1.4 V) to investigate the theoretical Ca^{2+} storage capacity of MVOH. Before the GITT test, the cell was activated by charge/discharge for five cycles. It displayed a theoretical discharge capacity of 149.4 mAh g^{-1} , corresponding to ~ 0.57 Ca^{2+} ion intercalation. To further investigate the reversible specific capacity and cycling stability, galvanostatic charge/

discharge testing was performed. All of the cells were aged for 10 h before the charge/discharge to ensure full infiltration of the electrolyte. As shown in Figure 2c, a reversible discharge capacity of $\sim 120 \text{ mAh g}^{-1}$ was obtained at 20 mA g^{-1} . Note that the first discharge capacity (corresponding to Ca^{2+} intercalation in MVOH) is obviously lower than that of the subsequent cycles, which is attributed to the spontaneous intercalation of slight Ca^{2+} ions into the structure during the aging process, as demonstrated in the following. The charge/discharge cycling at 50 mA g^{-1} is shown in Figure 2d. It shows stable cycling performance for 100 cycles with capacity retention of 106.4% relative to the second discharge capacity. The slight capacity increase may be attributed to activation of the electrode during cycling. To further demonstrate the cycling stability of MVOH for Ca^{2+} storage, long-term cycling performance was studied at 100 mA g^{-1} , as shown in Figure 2e. The second discharge capacity is 70.2 mAh g^{-1} , and a capacity retention of 86.9% after 500 cycles is displayed with

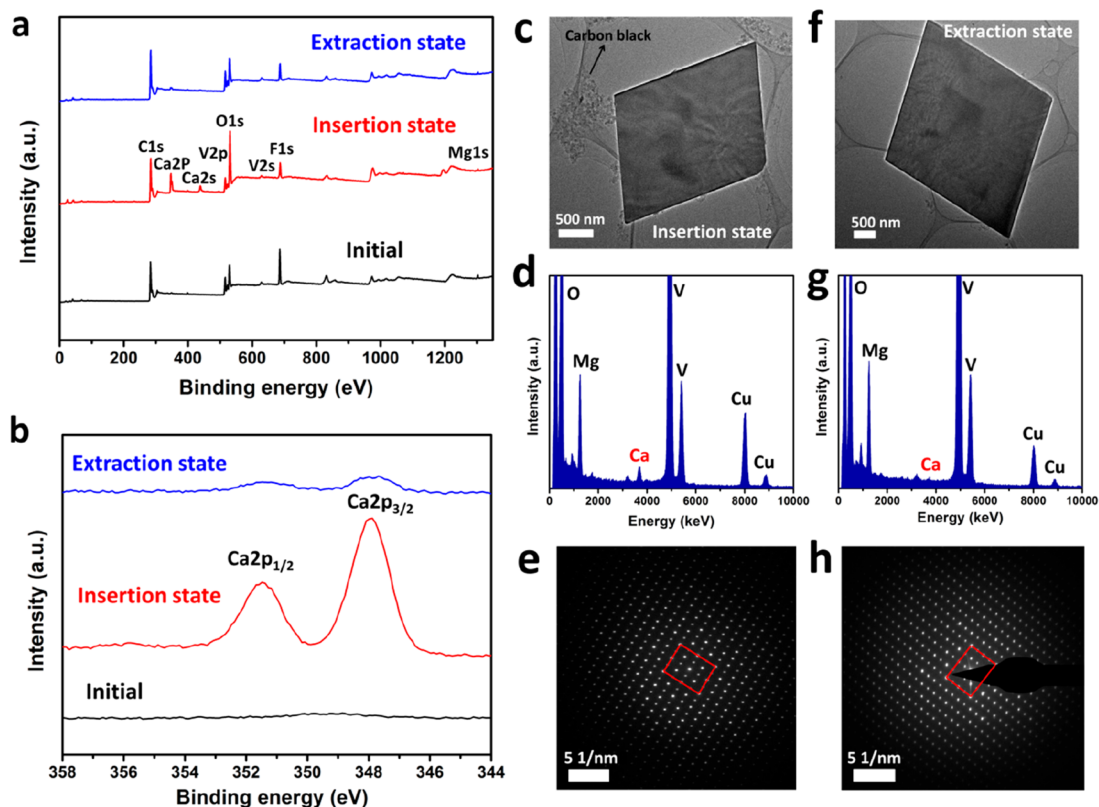


Figure 3. Element and structure characterizations of $\text{Mg}_{0.25}\text{V}_2\text{O}_5\cdot\text{H}_2\text{O}$ at Ca^{2+} insertion and extraction states. (a) XPS spectra of the electrodes at initial, insertion, and extraction states. (b) High-resolution Ca 2p spectra of the electrodes at initial, insertion, and extraction states. (c–e) TEM image (c), EDX spectrum (d), and SAED pattern (e) of $\text{Mg}_{0.25}\text{V}_2\text{O}_5\cdot\text{H}_2\text{O}$ at the Ca^{2+} insertion state. (f–h) TEM image (f), EDX spectrum (g), and SAED pattern (h) of $\text{Mg}_{0.25}\text{V}_2\text{O}_5\cdot\text{H}_2\text{O}$ at the Ca^{2+} extraction state.

Coulombic efficiency of over 98.4% during cycling (the first discharge was regarded as a precycle and was not taken into account when calculating the Coulombic efficiency). To the best of our knowledge, this is the best cycling performance among the reported Ca^{2+} storage cathodes (Table S1).^{22–30}

Since the Ca^{2+} storage performance of MVOH is investigated for the first time, it is very important and necessary to get deeper insights about the Ca^{2+} insertion/extraction process and the origin of its stable cycling performance. Ex situ XPS measurements were performed on the electrodes at the initial state (fresh electrode without any treatment), insertion state (discharge to -2.0 V), and extraction state (charge to 1.4 V). The cells at the insertion state and extraction state were disassembled immediately in the glovebox, and the electrodes were rinsed with alcohol several times to remove the electrolyte. It was found that the distinct Ca 2p and Ca 2s spectra are observed at the insertion state, compared to that at the initial state and extraction state (Figure 3a). For the high-resolution spectra of Ca 2p, there is no signal for the initial state, while two strong peaks at 351.5 and 347.9 eV are observed at the insertion state, corresponding to Ca 2p_{1/2} and Ca 2p_{3/2}, respectively (Figure 3b). At the extraction state, the Ca 2p_{1/2} and Ca 2p_{3/2} signals become very weak. These results manifest the reversible insertion/extraction of Ca^{2+} ions in the MVOH structure. The high-resolution spectra of Mg 1s and V 2p are shown in Figure S7. The Mg 1s signal shows no distinct change at the three states. For the V 2p spectra, two portions can be fitted at the initial state, corresponding to V^{5+} and V^{4+} (Figure S7b). At the Ca^{2+} insertion state, the V 2p spectra become widened, and another

portion corresponding to V^{3+} could be fitted (Figure S7d). Besides, the $\text{V}^{5+}/\text{V}^{4+}$ ratio decreased. At the Ca^{2+} extraction state, the V 2p spectra recovered and was similar to that at initial state (Figure S7f). The XPS results reveal that the Ca^{2+} insertion is accompanied by partial reduction of V^{5+} to V^{4+} and V^{4+} to V^{3+} , and the valence variation is reversible.

To investigate the effect of Ca^{2+} insertion/extraction on the structure of MVOH, ex situ TEM was carried out. Figure 3c–e shows the TEM, EDX, and SAED results of the Ca^{2+} insertion state of MVOH, while Figure 3f–h shows those of the Ca^{2+} extraction state. The morphology of the plates is maintained very well at both the insertion state and the extraction state, indicating good structural stability. The EDX spectrum shows a distinct signal corresponding to Ca at the insertion state (Figure 3d), which is almost gone at the extraction state (Figure 3g), consistent with the XPS results. SAED patterns at these two states displayed similar single-crystalline electron diffraction patterns (Figure 3e and 3h), suggesting that there is no distinct crystal structure change of MVOH during Ca^{2+} insertion and extraction.

Ex situ XRD measurements were performed to get further insight on the structural evolution of MVOH during charge/discharge. As shown in Figure 4a,b, the XRD patterns of the electrodes at six different states were collected. The XRD results at different states show similar patterns, revealing a minor structural change. Figure 4c–e displays zoom-in images of (001) peaks, (003) peaks, and diffraction peaks from Al foil. The peaks from Al foil at about 65° are consistent with each other in position at different states, which can be used as the internal standard. The (001) peak at about 8.2° , which is the

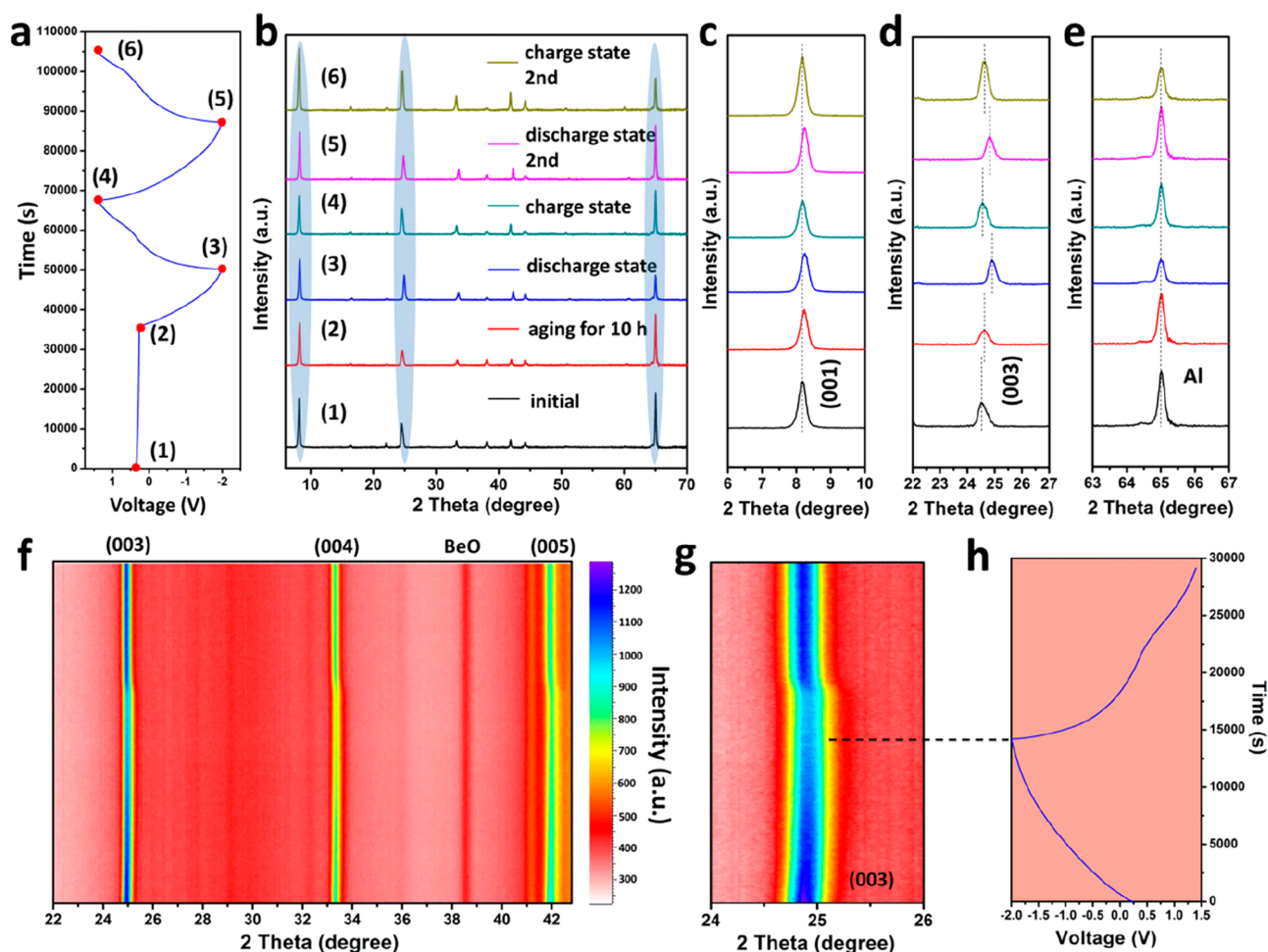


Figure 4. In situ/ex situ XRD characterizations of $\text{Mg}_{0.25}\text{V}_2\text{O}_5\cdot\text{H}_2\text{O}$ for Ca^{2+} storage. (a) Time–voltage curve at the initial stage. (b) Ex situ XRD patterns at six different states. (c–e) Zoom-in images of (b) for (001) peaks (c), (003) peaks (d), and Al peaks (e). (f) In situ XRD patterns during initial discharge and charge processes. (g) Zoom-in image of (f) for (003) peaks. (h) Corresponding discharge/charge profiles.

characteristic reflection of the layered structure, shows only a slight shift, which is even unobservable (Figure 4c). On the basis of the (003) peak (Figure 4d), the evolution regulation of the interlayer spacing can be observed more clearly because the variation of the (003) peak is three times that for (001) reflection. For the electrode after aging for 10 h, the (001) and (003) peaks shifted slightly toward high angle, indicating slight contraction of the interlayer spacing. Combined with the fact that the first discharge capacity is lower than that of subsequent cycles, it is believed that the slight contraction is caused by spontaneous intercalation of a small amount of Ca^{2+} ions into the interlayers during the aging process. For the electrode at the discharge state, further shifting of the (003) peak toward high angle was observed, indicating further contraction of the interlayer spacing as more Ca^{2+} ion insertion. The contraction can be attributed to the electrostatic interaction between the divalent Ca^{2+} ions and the oxygen on the surface of V–O layers. However, on the basis of the XRD results, the interlayer spacing only changed from ~ 10.77 Å at the initial state to ~ 10.68 Å at the discharge state and recovered to ~ 10.77 Å at the charge state. The whole layer spacing variation is only ~ 0.09 Å (± 0.02 Å) (change rate of $\sim 0.8\%$), and the small reversible variation was also confirmed at the second discharge and charge states. The ex situ XRD results demonstrate a tiny interlayer spacing variation and

excellent structural stability of MVOH during Ca^{2+} ion insertion and extraction, which reveals the origin of its superior cycling stability for Ca^{2+} storage.

In situ XRD measurement was also applied to further investigate the structural evolution of MVOH. As shown in Figure 4f, reflections corresponding to (003), (004), and (005) peaks were observed, which show unobservable variation during discharge and charge. From the zoom-in image of the (003) peak in Figure 4g, we found a slight shift with a decrease in intensity during discharge. There is no phase change in the whole discharge process, revealing single-phase solid solution reaction behavior of MVOH for Ca^{2+} storage. In the charge process, the (003) peak recovered to its original state for both the position and intensity. However, different from the gradual shift and weakening of the peak during discharge, immediate recovery during the charge process was observed (Figures 4g and S8), revealing the different structural evolution mechanism of MVOH during Ca^{2+} insertion and extraction processes, which explains the origin of the asymmetric redox reaction observed in the CV curve. Despite the asymmetric evolution feature, the in situ XRD results match very well with the ex situ XRD results and indicate a tiny structure change of MVOH during the Ca^{2+} insertion/extraction processes.

The tiny variation of the interlayer spacing enables MVOH to maintain superior structural stability and integrity in the

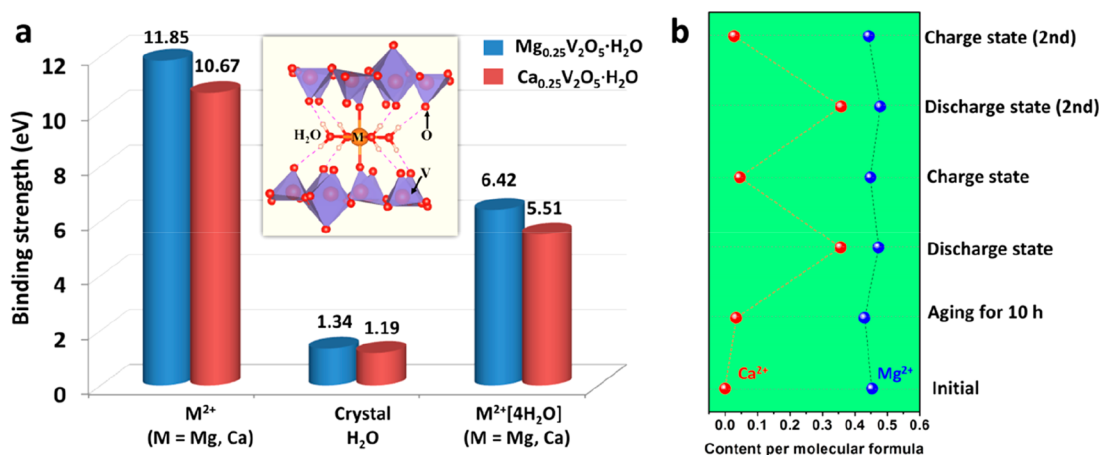


Figure 5. Comparison of the stability of Mg²⁺ and Ca²⁺ between the interlayers. (a) Calculated binding strengths of M²⁺ (M = Mg, Ca), crystal H₂O, and M²⁺[4H₂O] in the crystal Mg_{0.25}V₂O₅·H₂O; the inset is an illustration of the crystal model. (b) Content variation of Mg²⁺ and Ca²⁺ per molecular formula of Mg_{0.25}V₂O₅·H₂O at different charge/discharge states based on the ex situ ICP measurements.

long-term cycling. To confirm that, the XRD patterns of the electrodes after 50 cycles and 100 cycles were recorded (Figure S9), which are basically the same as that before cycling. The morphology of MVOH after 50 cycles was also investigated through ex situ SEM (Figure S10). As expected, the morphology with parallelogram-shaped plates is maintained well due to the tiny structural change in the charge/discharge processes. However, interestingly, a porous structure was observed on the edge of the plates, which should be caused by the intercalation and deintercalation of Ca²⁺ ions. The generated pores will effectively increase the diffusion kinetics of Ca²⁺ in the subsequent cycles, which explains the observed capacity increase, as shown in Figure 2d,e.

On the basis of the above in situ and ex situ characterizations, it is demonstrated that MVOH possesses an ultrastable bilayered structure with a slight change of interlayer spacing for Ca²⁺ storage. We believe that the stability of Mg²⁺ in the interlayers of MVOH plays a crucial role in the structural stability during Ca²⁺ insertion/extraction. With a smaller ionic size of Mg²⁺ ions compared to Ca²⁺ ions, Mg²⁺ shows larger charge density and thus stronger electrostatic interaction with the oxygen on the adjacent layers and oxygen in crystal water. The stronger electrostatic interaction will result in good stability of Mg²⁺ in the interlayers during Ca²⁺ insertion/extraction. Besides, the stable Mg²⁺ ions will effectively hold the crystal water in the interlayers due to the larger electrostatic force. Both the stable Mg²⁺ ions and crystal water will result in a solid pillared layered structure and thus excellent structural stability for Ca²⁺ storage.

To confirm our qualitative analysis, we quantitatively studied the stability of M²⁺ (M = Mg, Ca), crystal H₂O, and M²⁺[4H₂O] in the crystal Mg_{0.25}V₂O₅·H₂O using an ab initio approach. The calculated binding strengths of Mg²⁺ (11.85 eV), H₂O (1.34 eV), and Mg²⁺[4H₂O] (6.42 eV) in Mg_{0.25}V₂O₅·H₂O are all higher than those of Ca²⁺ (10.67 eV), H₂O (1.19 eV), and Ca²⁺[4H₂O] (5.51 eV) in Ca_{0.25}V₂O₅·H₂O, respectively (Figure 5a). The higher binding strength means better stability, demonstrating that Mg²⁺ is more stable while Ca²⁺ is easier to diffuse in the interlayers. Besides, the higher binding strength of H₂O in Mg_{0.25}V₂O₅·H₂O than that in Ca_{0.25}V₂O₅·H₂O indicates the stronger trapping effect of Mg²⁺ than Ca²⁺ on H₂O and thus suggests that the crystal water in Mg_{0.25}V₂O₅·H₂O is stable and will not

be brought out by Ca²⁺ ions during charge/discharge. The theoretical results provide deeper insight into the structural stability of MVOH for Ca²⁺ storage and further confirm our analysis above.

To further present the stability of Mg²⁺ and mobility of Ca²⁺ in the structure of MVOH, ex situ inductively coupled plasma (ICP) measurements (Figure S11) were performed to detect the molar ratio of Mg, Ca, and V in the electrodes at six different states (same as that in Figure 4a). As displayed in Table S2 and Figure 5b, the Mg/V ratios are 0.453/2 (initial state), 0.430/2 (aging for 10 h), 0.473/2 (discharge state), 0.448/2 (charge state), 0.478/2 (discharge state, second), and 0.443/2 (charge state, second). The Ca/V ratios are 0.001/2 (initial state), 0.034/2 (aging for 10 h), 0.356/2 (discharge state), 0.045/2 (charge state), 0.358/2 (discharge state, second), and 0.028/2 (charge state, second). The measured Mg/V ratios basically stay at a same level (Figure 5b), demonstrating the stability of Mg²⁺ in the structure. In comparison, the Ca/V ratios varied distinctly at different states (Figure 5b). Note that the Ca/V ratio changed from 0.001/2 at the initial state to 0.034/2 after aging for 10 h, manifesting that few Ca²⁺ ions inserted into the interlayers spontaneously during the aging process. At the discharge state, the Ca/V ratio was about 0.36/2. It indicates that ~0.36 Ca²⁺ intercalated per molecular formula in initial cycles, corresponding to a capacity of 93.7 mAh g⁻¹, which is basically consistent with the results obtained by electrochemical testing. At the charge state, the Ca/V ratios are 0.045/2 and 0.028/2, indicating that the Ca²⁺ ions are almost extracted with a trace remaining in the structure. The ICP results together with ab initio calculations manifest the stability of Mg²⁺ and mobility of Ca²⁺ in the interlayers of MVOH and explain the excellent structural stability of MVOH during Ca²⁺ intercalation/deintercalation.

Besides, it should be noted that the average Mg/V ratio detected by ICP is about 0.45/2, which is higher than the stoichiometric ratio of 0.25/2. The excess of Mg²⁺ in the structure could be attributed to the excessive addition of Mg source in the synthesis process (see details in the Supporting Information). The detailed impact of the excess Mg²⁺ on the performance needs further investigation. However, it is believed that the excess Mg²⁺ in the interlayers will occupy some active sites and result in decreased capacity. Therefore, we expect that a higher Ca²⁺ storage capacity for MVOH may

be realized with further regulation of the Mg/V ratio using an optimized synthesis route.

In summary, we identified bilayered $\text{Mg}_{0.25}\text{V}_2\text{O}_5\cdot\text{H}_2\text{O}$ with a large interlayer spacing of 10.76 Å as a stable cathode material for CIBs. On the basis of in situ/ex situ characterizations combined with ab initio calculations, the Mg^{2+} ions are demonstrated to be stable in the interlayers, while Ca^{2+} ions are diffusible during charge/discharge processes. The stable hydrated Mg^{2+} in the interlayers results in a solid pillared layered structure, with a tiny interlayer spacing variation of about 0.09 Å during the Ca^{2+} intercalation/deintercalation. Such an ultrastable structure enables $\text{Mg}_{0.25}\text{V}_2\text{O}_5\cdot\text{H}_2\text{O}$ to realize long-term cycling stability (500 cycles with capacity retention of 86.9%) for Ca^{2+} storage. Because investigations of CIBs are still at the initial stage, this work may lay an important foundation and open a new avenue for the identification of high-performance cathode materials for rechargeable CIBs.

■ ASSOCIATED CONTENT

Supporting Information

The Supporting Information is available free of charge on the ACS Publications website at DOI: 10.1021/acseenergylett.9b00830.

Experimental details; SEM, TGA, and XPS characterizations of the obtained material; CV curve of the ferrocene; ex situ XPS, ex situ XRD, ex situ SEM, and ex situ ICP measurements of the electrodes at different states; and zoom-in images of in situ XRD results (PDF)

■ AUTHOR INFORMATION

Corresponding Authors

*E-mail: mlq518@whut.edu.cn.

*E-mail: bsong@usst.edu.cn.

ORCID

Bo Song: 0000-0001-5600-106X

Liqiang Mai: 0000-0003-4259-7725

Author Contributions

*X.X. and M.D. contributed equally to this work.

Notes

The authors declare no competing financial interest.

■ ACKNOWLEDGMENTS

This work was supported by the National Natural Science Fund for Distinguished Young Scholars (51425204), the National Natural Science Foundation of China (51832004, 51521001, 11404230), the National Key Research and Development Program of China (2016YFA0202601), the Programme of Introducing Talents of Discipline to Universities (B17034), and the Yellow Crane Talent (Science & Technology) Program of Wuhan City.

■ REFERENCES

- (1) Muldoon, J.; Bucur, C. B.; Gregory, T. Quest for nonaqueous multivalent secondary batteries: magnesium and beyond. *Chem. Rev.* **2014**, *114* (23), 11683–11720.
- (2) Canepa, P.; Sai Gautam, G.; Hannah, D. C.; Malik, R.; Liu, M.; Gallagher, K. G.; Persson, K. A.; Ceder, G. Odyssey of multivalent cathode materials: open questions and future challenges. *Chem. Rev.* **2017**, *117* (5), 4287–4341.
- (3) Zhou, L.; Liu, Q.; Zhang, Z.; Zhang, K.; Xiong, F.; Tan, S.; An, Q.; Kang, Y.-M.; Zhou, Z.; Mai, L. Interlayer-Spacing-Regulated VOPO_4 Nanosheets with Fast Kinetics for High-Capacity and

Durable Rechargeable Magnesium Batteries. *Adv. Mater.* **2018**, *30*, 1801984.

- (4) Xu, Y.; Deng, X.; Li, Q.; Zhang, G.; Xiong, F.; Tan, S.; Wei, Q.; Lu, J.; Li, J.; An, Q.; Mai, L. Vanadium Oxide Pillared by Interlayer Mg^{2+} Ions and Water as Ultralong-Life Cathodes for Magnesium-Ion Batteries. *Chem.* **2019**, *5*, 1194.

- (5) Attias, R.; Salama, M.; Hirsch, B.; Pant, R.; Gofer, Y.; Aurbach, D. Anion Effects on Cathode Electrochemical Activity in Rechargeable Magnesium Batteries: A Case Study of V_2O_5 . *ACS Energy Lett.* **2019**, *4* (1), 209–214.

- (6) Kundu, D.; Adams, B. D.; Duffort, V.; Vajargah, S. H.; Nazar, L. F. A high-capacity and long-life aqueous rechargeable zinc battery using a metal oxide intercalation cathode. *Nat. Energy* **2016**, *1* (10), 16119.

- (7) Ming, F.; Liang, H.; Lei, Y.; Kandambeth, S.; Eddaoudi, M.; Alshareef, H. N. Layered $\text{Mg}_x\text{V}_2\text{O}_5\cdot n\text{H}_2\text{O}$ as cathode material for high-performance aqueous zinc ion batteries. *ACS Energy Lett.* **2018**, *3*, 2602–2609.

- (8) Ding, J.; Du, Z.; Gu, L.; Li, B.; Wang, L.; Wang, S.; Gong, Y.; Yang, S. Ultrafast Zn^{2+} intercalation and deintercalation in vanadium dioxide. *Adv. Mater.* **2018**, *30* (26), 1800762.

- (9) Zhang, N.; Dong, Y.; Jia, M.; Bian, X.; Wang, Y.; Qiu, M.; Xu, J.; Liu, Y.; Jiao, L.; Cheng, F. Rechargeable Aqueous Zn– V_2O_5 Battery with High Energy Density and Long Cycle Life. *ACS Energy Lett.* **2018**, *3* (6), 1366–1372.

- (10) Lin, M. C.; Gong, M.; Lu, B.; Wu, Y.; Wang, D. Y.; Guan, M.; Angell, M.; Chen, C.; Yang, J.; Hwang, B. J.; Dai, H. An ultrafast rechargeable aluminium-ion battery. *Nature* **2015**, *520* (4), 324–328.

- (11) Li, C.; Dong, S.; Tang, R.; Ge, X.; Zhang, Z.; Wang, C.; Lu, Y.; Yin, L. Heteroatomic interface engineering in MOF-derived carbon heterostructures with built-in electric-field effects for high performance Al-ion batteries. *Energy Environ. Sci.* **2018**, *11* (11), 3201–3211.

- (12) Elia, G. A.; Marquardt, K.; Hoepfner, K.; Fantini, S.; Lin, R.; Knipping, E.; Peters, W.; Drillet, J. F.; Passerini, S.; Hahn, R. An overview and future perspectives of aluminum batteries. *Adv. Mater.* **2016**, *28* (35), 7564–7579.

- (13) Gummow, R. J.; Vamvounis, G.; Kannan, M. B.; He, Y. Calcium-ion batteries: Current state-of-the-art and future perspectives. *Adv. Mater.* **2018**, *30* (39), 1801702.

- (14) Wang, Y.; Chen, R.; Chen, T.; Lv, H.; Zhu, G.; Ma, L.; Wang, C.; Jin, Z.; Liu, J. Emerging non-lithium ion batteries. *Energy Storage Mater.* **2016**, *4*, 103–129.

- (15) Gheyhani, S.; Liang, Y.; Wu, F.; Jing, Y.; Dong, H.; Rao, K.; Chi, X.; Fang, F.; Yao, Y. An aqueous Ca-ion battery. *Adv. Sci.* **2017**, *4* (12), 1700465.

- (16) Yabuuchi, N.; Kubota, K.; Dahbi, M.; Komaba, S. Research development on sodium-ion batteries. *Chem. Rev.* **2014**, *114* (23), 11636–11682.

- (17) Ponrouch, A.; Palacin, M. R. On the road toward calcium-based batteries. *Current Opinion in Electrochemistry* **2018**, *9*, 1–7.

- (18) Ponrouch, A.; Frontera, C.; Bardé, F.; Palacin, M. R. Towards a calcium-based rechargeable battery. *Nat. Mater.* **2016**, *15* (2), 169–172.

- (19) Wang, D.; Gao, X.; Chen, Y.; Jin, L.; Kuss, C.; Bruce, P. G. Plating and stripping calcium in an organic electrolyte. *Nat. Mater.* **2018**, *17* (1), 16–20.

- (20) Wang, M.; Jiang, C.; Zhang, S.; Song, X.; Tang, Y.; Cheng, H. M. Reversible calcium alloying enables a practical room-temperature rechargeable calcium-ion battery with a high discharge voltage. *Nat. Chem.* **2018**, *10* (6), 667–672.

- (21) Wu, S.; Zhang, F.; Tang, Y. A novel calcium-ion battery based on dual-carbon configuration with high working voltage and long cycling life. *Adv. Sci.* **2018**, *5* (8), 1701082.

- (22) Lipson, A. L.; Pan, B.; Lapidus, S. H.; Liao, C.; Vaughey, J. T.; Ingram, B. J. Rechargeable Ca-ion batteries: A new energy storage system. *Chem. Mater.* **2015**, *27*, 8442–8447.

- (23) Padigi, P.; Goncher, G.; Evans, D.; Solanki, R. Potassium barium hexacyanoferrate – A potential cathode material for

rechargeable calcium ion batteries. *J. Power Sources* **2015**, *273* (273), 460–464.

(24) Shiga, T.; Kondo, H.; Kato, Y.; Inoue, M. Insertion of Calcium Ion into Prussian Blue Analogue in Nonaqueous Solutions and Its Application to a Rechargeable Battery with Dual Carriers. *J. Phys. Chem. C* **2015**, *119* (50), 27946–27953.

(25) Tojo, T.; Sugiura, Y.; Inada, R.; Sakurai, Y. Reversible calcium ion batteries using a dehydrated prussian blue analogue cathode. *Electrochim. Acta* **2016**, *207*, 22–27.

(26) Cabello, M.; Nacimiento, F.; González, J. R.; Ortiz, G.; Alcántara, R.; Lavela, P.; Pérez-Vicente, C.; Tirado, J. L. Advancing towards a veritable calcium-ion battery: CaCo_2O_4 positive electrode material. *Electrochem. Commun.* **2016**, *67*, 59–64.

(27) Lipson, A. L.; Kim, S.; Pan, B.; Liao, C.; Fister, T. T.; Ingram, B. J. Calcium intercalation into layered fluorinated sodium iron phosphate. *J. Power Sources* **2017**, *369*, 133–137.

(28) Kuperman, N.; Padigi, P.; Goncher, G.; Evans, D.; Thiebes, J.; Solanki, R. High performance Prussian Blue cathode for nonaqueous Ca-ion intercalation battery. *J. Power Sources* **2017**, *342*, 414–418.

(29) Vo, T. N.; Kim, H.; Hur, J.; Choi, W.; Kim, I. T. Surfactant-assisted ammonium vanadium oxide as a superior cathode for calcium-ion batteries. *J. Mater. Chem. A* **2018**, *6*, 22645–22654.

(30) Cabello, M.; Nacimiento, F.; Alcántara, R.; Lavela, P.; Pérez Vicente, C.; Tirado, J. L. Applicability of Molybdate as an Electrode Material in Calcium Batteries: A Structural Study of Layer-type Ca_xMoO_3 . *Chem. Mater.* **2018**, *30* (17), 5853–5861.

(31) Sai Gautam, G.; Canepa, P.; Richards, W. D.; Malik, R.; Ceder, G. Role of structural H_2O in intercalation electrodes: the case of Mg in nano-crystalline Xerogel- V_2O_5 . *Nano Lett.* **2016**, *16* (4), 2426–2431.

(32) Yan, M.; He, P.; Chen, Y.; Wang, S.; Wei, Q.; Zhao, K.; Xu, X.; An, Q.; Shuang, Y.; Shao, Y.; et al. Water-lubricated intercalation in $\text{V}_2\text{O}_5 \cdot n\text{H}_2\text{O}$ for high-capacity and high-rate aqueous rechargeable zinc batteries. *Adv. Mater.* **2018**, *30* (1), 1703725.

(33) Oka, Y.; Yao, T.; Yamamoto, N. Crystal Structures and Lattice Distortions of σ -Type Layered Vanadium Bronzes: $\sigma\text{-M}_{0.25}\text{V}_2\text{O}_5 \cdot \text{H}_2\text{O}$ ($M = \text{Mg}, \text{Co}, \text{Ni}$). *J. Solid State Chem.* **1999**, *144*, 181–187.

(34) Lipson, A. L.; Proffit, D. L.; Pan, B.; Fister, T. T.; Liao, C.; Burrell, A. K.; Vaughney, J. T.; Ingram, B. J. Current Collector Corrosion in Ca-Ion Batteries. *J. Electrochem. Soc.* **2015**, *162* (8), A1574–A1578.

(35) Murata, Y.; Takada, S.; Obata, T.; Tojo, T.; Inada, R.; Sakurai, Y. Effect of water in electrolyte on the Ca^{2+} insertion/extraction properties of V_2O_5 . *Electrochim. Acta* **2019**, *294*, 210–216.

(36) Tojo, T.; Tawa, H.; Oshida, N.; Inada, R.; Sakurai, Y. Electrochemical characterization of a layered $\alpha\text{-MoO}_3$ as a new cathode material for calcium ion batteries. *J. Electroanal. Chem.* **2018**, *825*, 51–56.